NeuroImage 46 (2009) 958–966

Contents lists available at ScienceDirect

NeuroImage

journal homepage: www.elsevier.com/locate/ynimg

In vivo evidence for the selective subcortical degeneration in Huntington's disease

Gwenaëlle Douaud [a,b,*], Timothy E. Behrens [b], Cyril Poupon [c], Yann Cointepas [c], Saâd Jbabdi [b], Véronique Gaura [a], Narly Golestani [d], Pierre Krystkowiak [e], Christophe Verny [f], Philippe Damier [g], Anne-Catherine Bachoud-Lévi [h,i], Philippe Hantraye [a], Philippe Remy [a,i]

[a] *URA CEA-CNRS 2210, SHFJ, Orsay, France*
[b] *FMRIB Centre, Department of Clinical Neurology, University of Oxford, OX39DU Oxford, UK*
[c] *Neurospin, Gif-sur-Yvette, France*
[d] *Department of Clinical Neurosciences, University Medical School, Geneva, Switzerland; Institute of Cognitive Neuroscience, University College, London, UK*
[e] *Service de Neurologie, CHU Amiens, France*
[f] *Département de Neurologie, CHU Angers, France*
[g] *INSERM CIC0004 UMR643; CHU Nantes, Clinique Neurologique, France*
[h] *INSERM U421/Ecole Normale Supérieure, Paris; CHU Henri Mondor, Créteil, France*
[i] *Département de Neurosciences cliniques, CHU Henri Mondor, AP-HP, Paris XII, France*

ARTICLE INFO

Article history:
Received 8 January 2009
Revised 4 March 2009
Accepted 18 March 2009
Available online 28 March 2009

Keywords:
Huntington's disease
Basal ganglia
Diffusion tensor imaging
Increased fractional anisotropy
Principal diffusion direction

ABSTRACT

Although Huntington's disease is largely considered to be a subcortical disease, there is no clear consensus on whether all deep grey matter loss is a direct downstream consequence of the massive degeneration of the medium-size spiny neurons in the striatum. Our aim was to characterise *in vivo* such preferential degeneration by analysing various distinct diffusion imaging measures including mean diffusivity, anisotropy, fibre orientation (using the information of the principal diffusion direction) and white matter tractography. All results converged to demonstrate the selective degeneration of connections in subcortical grey and white matter, degeneration which was likely to originate with the death of the striatal medium-size spiny neurons. Indeed, we found a significant increase of MD and FA in all the subcortical grey matter structures involved in the cortico-striato-thalamo-cortical loops. The atypical striatal and pallidal increase of FA was concurrent to a decrease of the dispersion of the fibre orientation, unambiguously characterising a preferential loss of connections along specific radiating directions from these structures while some others are comparatively spared. Analysis of striatal and pallidal white matter tracts revealed that striato-pallidal projections were the most affected. The ability of DTI to uncover the impact of such neurodegenerative disease on some specific neuronal/axonal populations is a further step towards the future definition of a surrogate marker of this disease. Beyond Huntington's disease, we prove here that diffusion imaging technique, associated to adequate methodological analyses, can provide insight into any neurodegenerative disorder for which some neuronal populations or connections are selectively targeted over others.

Introduction

Huntington's disease (HD) is a lethal autosomic dominant neurodegenerative disease that predominantly affects subcortical grey matter structures. *Post mortem*, it is characterised at the cellular level by the progressive degeneration of the striatal medium-size spiny neurons, which represent the great majority of the neuronal populations of the striatum (Graveland et al., 1985; Vonsattel et al., 1985). *In vivo*, the subcortical impact of HD is macroscopically depicted by the atrophy of the striatum, the pallidum and the thalamus–referred to hereafter as the "subcortical grey nuclei" or SGN–but also of the substantia nigra as measured by conventional structural MRI (Jernigan et al., 1991; Aylward et al., 2004; Fennema-Notestine et al., 2004; Douaud et al., 2006).

It remains unclear whether all deep grey matter loss can be attributed to the original death of striatal spiny neurons. The primary degeneration in the striatum may spread to the other subcortical nuclei composing the basal ganglia loops via the preferential loss of striato-pallidal projections. Being able to characterise such preferential degeneration in basal ganglia connections would be crucial to determine whether protecting or replacing striatal cells would be enough to prevent extrastriatal cell loss (Bachoud-Levi et al., 2000; McBride et al., 2006). Nevertheless, this question has never been addressed *in vivo* before and, contrary to *post mortem* investigations, would benefit from access to data at an early stage of the disease, permit a whole-brain

Abbreviations: HD, Huntington's disease; DTI, diffusion tensor imaging; FA, fractional anisotropy; MD, mean diffusivity; PDD, principal diffusion direction; ROI, region of interest; SGN, subcortical grey nuclei.

* Corresponding author. FMRIB Centre, Department of Clinical Neurology, University of Oxford, OX39DU Oxford, UK. Fax: +44 1865 222717.
E-mail address: douaud@fmrib.ox.ac.uk (G. Douaud).

1053-8119/$ – see front matter © 2009 Elsevier Inc. All rights reserved.
doi:10.1016/j.neuroimage.2009.03.044

exploration of the pathophysiological process and offer a unique way to monitor its progression and the effect of experimental treatments. However, this is not a question that can be answered by conventional imaging techniques. Indeed, these techniques are unable to distinguish regional brain atrophy that is general or non-specific in its cellular targets from atrophy that affects specific cell populations.

On the contrary, we hypothesised that diffusion tensor imaging (DTI) would have the potential to make such a distinction in cases where the connections of different populations of neurons have different orientational organization. First, mean diffusivity (MD) tends to be increased in pathological tissue–grey or white matter–where the density of cellular membranes is reduced. In tissue that is preferentially organized along a particular orientation, such as along axonal fibres, fractional anisotropy (FA) is commonly found to be decreased in case of a pathological process as a result of the reduction in cellular boundaries that hinder diffusion (Pierpaoli and Basser, 1996; Beaulieu, 2002). No systematic effect is observed on the main orientation of the underlying tissue, represented in practice by the orientation of the first eigenvector of the tensor (also called principal diffusion direction or PDD). However in deep grey matter, where there are multiple populations of cells and connections with different orientational preferences, a selective degeneration of *some* of these connections would make this tissue appear less isotropic, which corresponds to an atypical *increase* of FA. Subsequently, this preferential degeneration would also be characterised by a better coherence of these multiple orientations within these structures, i.e. by a decrease in the spatial dispersion of the PDD. A systematic shift of orientation of the PDD away from the more vulnerable connections should also be seen (Pierpaoli et al., 2001).

In HD, if the loss of subcortical grey matter originates from the death of medium-size spiny neurons in the striatum, then one organized population of neurons and axons should be comparatively more affected than the others. We thus would expect to see an increase in MD in deep grey matter structures as a marker of degeneration, accompanied by an increase in FA as evidence for the selectivity of this degeneration. Concurrently, fibre orientations should be spatially distributed more homogeneously, i.e. we should be able to show a decrease in their dispersion. In the putamen for instance, where connections to the pallidum (medio-lateral orientation) should degenerate more rapidly than the cortico-subcortical projections (dorso-ventral direction), we should be able to demonstrate a systematic change in fibre orientation towards this superior/inferior axis. Some selectivity in the degeneration of subcortical white matter tracts would also be expected. That is, for each subcortical structure, its connections (reconstructed using tractography) that would be directly affected by the initial death of striatal spiny neurons should be found more abnormal than the others.

HD therefore here serves as an exceptional pathological model to assess whether DTI technique combined to a specific methodology will be able to demonstrate a selective degeneration. This would clearly be of benefit for a better understanding and monitoring of other neurodegenerative diseases such as multiple sclerosis, in which an increase of FA in the basal ganglia was first witnessed (Ciccarelli et al., 2001).

Materials and methods

This study was part of the MIG-HD (Multicentric Intracerebral Grafting in HD) protocol and was approved by the ethics committee of Henri Mondor Hospital in Créteil. All subjects gave their written informed consent.

Subjects

14 HD patients (5 women, 9 men, aged 42 ± 8) were included in this study. All patients had a genetically proven HD with an abnormal number of CAG repeats ranging from 41 to 57 and at least 1 year of clinical symptoms. At the time of the imaging study, the majority of the patients ($n = 9$) were at stage I of the disease (total functional capacity or TFC = 11–13; Shoulson and Fahn, 1979). Four of the patients were at stage II (TFC = 10) and one was at stage III (TFC = 6). 10 control subjects (5 women, 5 men, aged 37 ± 12) underwent the same imaging protocol. We did not try to match patient and control populations for age. Indeed, we expected a differential impact of age on our DTI measures in the two groups which we controlled for statistically (see the Statistical analysis section below). Finally, HD patients were examined using the Unified Huntington's Disease Rating Scale (UHDRS) (1996) in each hospital and the scores for each subscale (motor, behavioural, functional and neuropsychological) were collected.

Data acquisition

Whole-brain T1-weighted and diffusion-weighted MRI were performed in all subjects using a 1.5T Signa Lx Echospeed imager (General Electric Healthcare, Milwaukee, WI) with 40 $mT.m^{-1}$ gradient capability and a standard bird-cage head coil. T1-weighted images were acquired with an improved 3D IR-FSPGR sequence that enhanced grey-white matter contrast (Douaud et al., 2006) using the following parameters: axial orientation, matrix 256×256, 124 slice locations, 0.9375×0.9375 mm^2 in-plane resolution, slice thickness 1.2 mm, TI/TE/TR = 620/2/20.3 ms, flip angle $\alpha = 10°$, read bandwidth RBW = 7.81 kHz.

Diffusion-weighted images were obtained using standard Stejskal–Tanner echo-planar sequence (Stejskal and Tanner, 1965) with axial orientation, matrix 128×128 interpolated to 256×256, 0.9375×0.9375 mm^2 in-plane resolution, slice thickness 2 mm, TE/TR = 71/2500 ms, 60 slices, $\alpha = 90°$, RBW = 125 kHz. A set of 41 orientations uniformly distributed over a sphere of radius $b = 700$ $s.mm^{-2}$ was used for the diffusion-sensitising gradients, and one T2-weighted image with no diffusion sensitisation ($b = 0$ $s.mm^{-2}$) was also acquired.

Image processing

Diffusion-weighted images of patients and controls were preprocessed in BrainVISA (Cointepas et al., 2001), which corrects for the echoplanar distortion (Mangin et al., 2002) and automatically extracts the diffusion tensor in each voxel.

In order to be confident in our findings, we carried out two independent analyses of the diffusion images. We first performed whole-brain voxel-wise analyses, which requires no *a priori* hypotheses regarding the location of the changes. These allowed us to discern whether the effects were specific to the deep grey matter structures. We then manually defined anatomical regions of interest (ROI) of the subcortical grey matter on a subject-by-subject basis, to ensure that any effect seen in the voxel-wise analyses could not be explained by a residual misregistration of the patient data to the standard space.

Preprocessing of FA, MD and |x|, |y| and |z| components of the PDD images for the voxel-wise analyses

Special care was given to the voxel-wise approach employed to register all MD and FA maps into a common standard space. Such an approach is delicate in Huntington's disease and the registration step may not correctly handle the massive atrophy of the deep grey nuclei, leading to a misinterpretation of the results (Douaud et al., 2006).

In a preliminary analysis using the SPM2 software (Wellcome Department of Cognitive Neurology, London), we found that the use of a template built from the b_0 images did not give a satisfactory realignment of the subcortical structures, probably due to the lack of contrast in these structures in such maps. Similarly, the use of a template of grey matter, constructed with the corresponding grey matter segmented T1-weighted images, happened to be insufficient to properly realign the subcortical structures. Indeed, diffusion-weighted images exhibit distortions due to susceptibility artefacts that are not

present in T1-weighted images and are, unfortunately, mainly located around the deep grey matter (Jezzard and Balaban, 1995; see Fig. S1 of the Supplementary material).

We therefore created a left–right symmetric study-specific FA template, in which the subcortical contrast is excellent, particularly in the anterior limb of the internal capsule that is crucial for properly realigning the caudate nucleus and the putamen. This FA template was built from the 10 control subjects and a subset of 10 patients (5 randomly chosen stage I patients, the 4 stage II patients and the patient at stage III). This discards the bias that would have resulted from favouring one of the two groups in the spatial normalisation step. To create this template, all the b_0 images, as well as their respective mirror images, were first realigned onto the ICBM 152 T2 template (MNI), which was masked to extract only brain information. Then, the non-linear parameters estimated from these registrations were applied to each native FA map and its mirror image. A mean image of the 20 FA normalised images and their 20 corresponding mirror images was created and then convolved with an isotropic 6 mm FWHM Gaussian kernel. All native FA maps were then non-linearly normalised onto this FA template and smoothed with a 6 mm FWHM Gaussian kernel (as the FWHM should be similar to the spatial extent of patient–control differences that are expected to be the strongest in the basal ganglia; Jones et al., 2005). The resulting non-linear transformations were applied to the MD maps (in which we removed the non-informative CSF signal) and to the maps of $|x|$, $|y|$ and $|z|$ projections of the first eigenvector of the diffusion tensor (PDD) in each voxel. Spatially normalised MD images as well as spatially normalised $|x|$, $|y|$ and $|z|$ maps of the PDD were then smoothed with a 6 mm FWHM Gaussian kernel.

Preprocessing of white matter images

We followed the optimised VBM protocol for the white matter images obtained from the segmentation of the corresponding T1-weighted images (Good et al., 2001). It was based on the creation of a symmetric study-specific template of white matter (the same 10 controls and 10 patients than for the diffusion voxel-based analyses) to which all the 24 native white matter segmented T1-weighted images were non-linearly registered. The modulated spatially normalised white matter images were smoothed with an isotropic 6 mm FWHM Gaussian kernel.

Creation of the anatomical ROI

We manually delineated the outlines of the entire striatum, pallidum and thalamus on the T1-weighted sequence of each brain. The striatum was further subdivided into the head and body of the caudate nucleus, the anterior and posterior putamen, and the ventral striatum. In order to do reliable identification of these anatomical ROIs, a single examiner (GD) segmented these deep brain nuclei in the T1-weighted images which were rigidly reoriented so that the anterior and posterior commissures were located in the same axial plane and the inter-hemispheric plane was perpendicular to this axial plane (the "AC-PC" space, the MNI152 space with no scaling factor; see Douaud et al., 2006 for more details on the delineation of the structures) (Fig. 1).

All diffusion-weighted images, including the PDD maps, were similarly reoriented in the AC-PC space with a rigid spatial transformation (the gradients directions were reoriented using the same transformation prior to the estimation of the tensor). To obtain MD and FA subcortical values in these various subregions, the ROI were then placed on MD and FA scans rigidly reoriented in each subject own AC-PC space, after being eroded by 1 mm to limit partial volume effects in diffusion index values. Finally, to correct for the subcortical distortions that can be more prominent in some subjects than others (Jezzard and Balaban, 1995), a translation was manually applied on a structure-by-structure and subject-by-subject basis, when some of the ROI were still not properly superimposed to the corresponding structure in the diffusion space.

Dispersion of the principal diffusion direction

We extracted in each voxel the information related to the first eigenvector of the diffusion tensor. Using the anatomical eroded ROI, we then calculated the dispersion of this PDD within each structure of the SGN following the recommendations of Schwartzman et al. (2005). In other words, we considered for each subject the orientation of the PDD in every voxel composing each ROI. We then calculated the value of the dispersion of the PDDs inside each subject's ROI (ranging from 0 for a perfect alignment of the PDDs across voxels to 2/3 for orientations completely randomly distributed) and finally compared it across groups.

Regularised streamline tractography

Each eroded ROI was finally also used as a seed mask for regularized streamline tractography (Perrin et al., 2005) using the following parameters: 1000 possible directions over a sphere, 40° for the solid angle of the cone of possible directions (so 56 possible directions within this cone), 0.47 mm step, mask defined by FA>0.15. This method determines the most probable direction to progress from one voxel to another by taking into account both the incident direction of the particle that reconstructs the virtual fibre and the principal diffusion direction derived from the tensor model. By attributing a weight to the incident direction of the particle that is larger in less anisotropic tissue, this tractography approach avoids a particle from being attracted to an improbable direction when it reaches a region of crossing fibres, such as the descending pathways from the sensorimotor cortex and the corpus callosum.

The virtual fibre tracts reconstructed for each subject were then fragmented and re-labeled: for instance, for two ROI A and B used as seed masks, we differentiated tracts joining ROI A and B from tracts going to or starting from ROI A and not joining ROI B and vice-versa (see Fig. S2 of the Supplementary material). For each SGN, it further follows from our hypotheses that the pathways directly affected by the death of medium-size spiny neurons of the striatum (striatum-

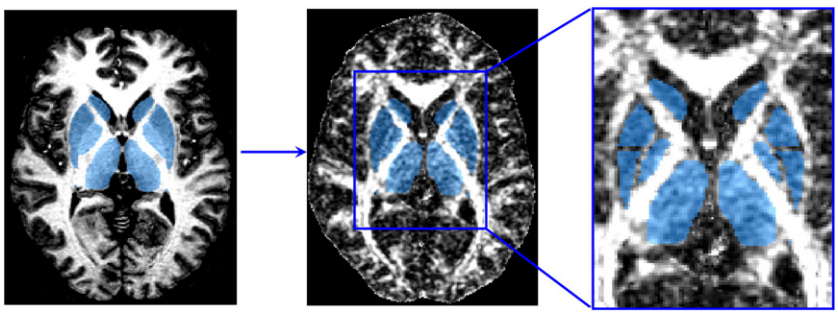

Fig. 1. Regions of interest in the SGN. Left: superimposition (in blue) of the manual delineation of the outlines of the striatum, the globus pallidus and the thalamus onto the improved T1 MRI. Middle and right: the same ROI before and after erosion superimposed onto the corresponding FA map.

pallidum) should demonstrate greater abnormalities than any other, comparatively more spared, known connections of this SGN (cortex-striatum, striatum-substantia nigra, thalamus-striatum; see Table S1 of the Supplementary material for details of these connections).

Statistical analysis

Voxel-wise analyses

The preprocessed maps of MD, FA and $|x|$, $|y|$ and $|z|$ components of the PDD were compared in SPM2, using the framework of the general linear model. Region-specific differences between the HD patients and controls were assessed with an ANCOVA, used to rule out the probable confounding effects of age and gender on the data. A diagnosis (controls/patients) by age interaction was also added in the model to investigate probable age-dependant differences between controls and patients (Fig. S3 of the Supplementary material). All the data was checked for normality. *P*-values were fully corrected for multiple comparisons using the false discovery rate (FDR) (Genovese et al., 2002). The significance level was set at $P<0.01$ FDR-corrected ($t>3.81$ for 19 DOF) for the MD maps analysis, $P<0.05$ FDR-corrected ($t>3.69$) for the FA maps analysis and finally at $P<0.05$ FDR-corrected ($t>4.25$) for $|x|$, $|y|$ and $|z|$ component maps of the PDD analyses. As we had a prior hypothesis about regional pathology in the subcortical grey matter, the same analyses were also limited to a set of spatially normalised ROI in the SGN for MD and FA analyses using the Marsbar toolbox in SPM2.

ROI analyses

Using statistical software Datamind (Duchesnay et al., 2004), the same ANCOVA with age, gender and diagnosis × age as confounding covariates was carried out to compare the values of mean MD, mean FA and dispersion of the PDD in each ROI between the patients and the controls. We also used the same statistical model to investigate MD in the subdivided virtual tracts. The age by diagnosis (controls/patients) interaction used in this model was relevant indeed as age happened to have a different impact on FA and MD in the subcortical grey matter between the two populations (see Fig. S4 of the Supplementary material). All the data was checked for normality. *P*-values less than 0.05 were considered significant.

Results

Whole-brain and ROI investigation of MD and FA: a first step towards the evidence of selective degeneration in the SGN

We found a significant increase in MD in the HD patients primarily located in the subcortical grey matter. More precisely, higher MD values were found bilaterally in the anterior and posterior putamen, the pallidum, the ventral striatum and the thalamus (centro-median nucleus and right ventro-lateral nucleus) (Fig. 2). Additional increase of MD was found in the corona radiata, more precisely in the frontal and parietal white matter, mainly around the central sulcus. All the

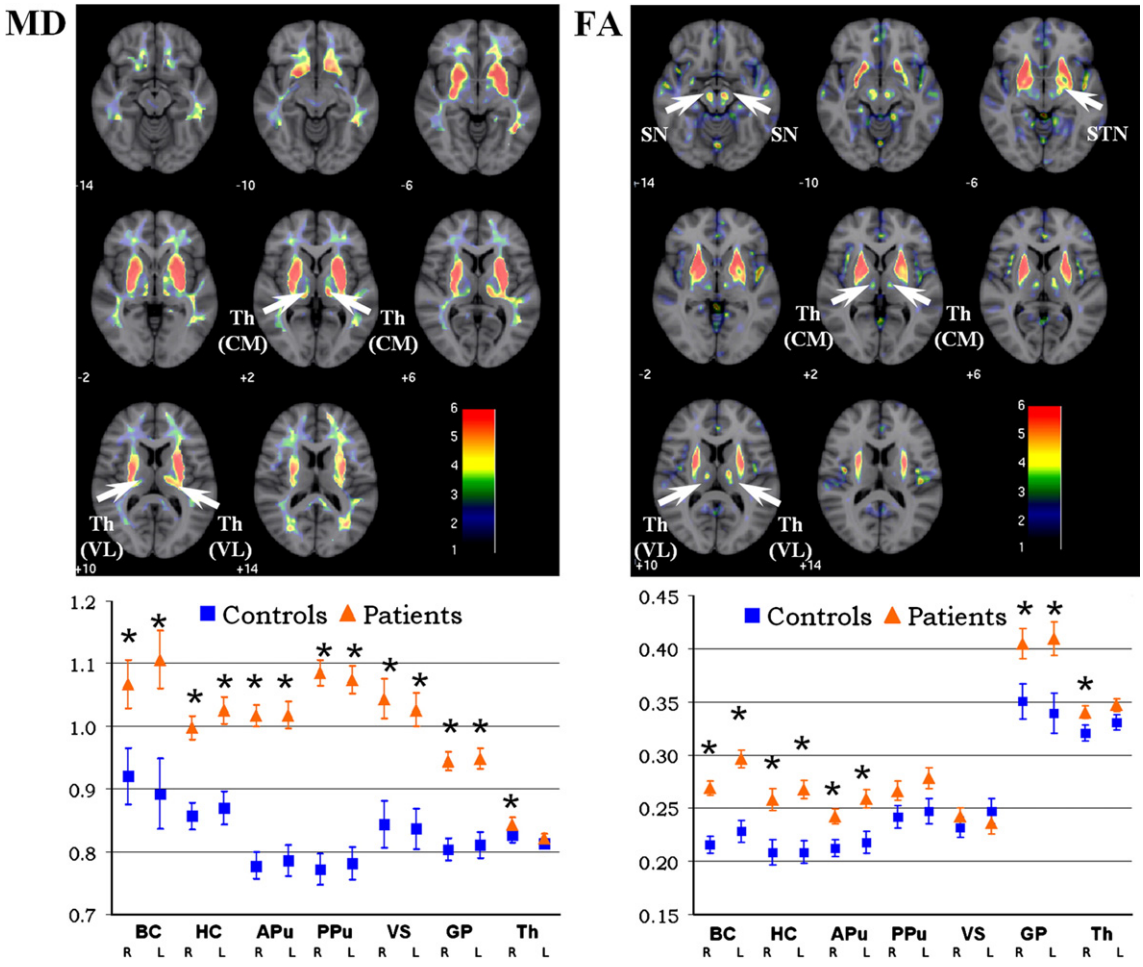

Fig. 2. Increase of MD (left) and FA (right) in the HD patients: voxel-wise and ROI ANCOVA results. The voxel-wise ANCOVA *t*-maps of MD and FA show significant increases almost exclusively confined to the subcortical grey matter of the patients. Arrows point at the thalamic nuclei (ventro-lateral and centro-median), the right subthalamic nucleus and the substantia nigra (left is left). The ROI analysis of adjusted (for confounding variables effect) mean MD ($\times 10^{-9}$ m^2.s^{-1}) and mean FA values ($\pm$SE) also show an increase in both DTI indices inside the SGN. BC = body of the caudate; HC = head of the caudate; APu = anterior putamen; PPu = posterior putamen; VS = ventral striatum; GP = globus pallidus; Th = thalamus. * = significant (see Table 3 and 4 of the Supplementary material).

significant results found in the statistical ANCOVA *t*-map are listed in Table S2 of the Supplementary material.

We also found significantly higher FA values in the HD patients almost exclusively confined to the subcortical grey matter, particularly bilaterally in the putamen, the pallidum, the ventral striatum, the thalamus (ventro-lateral nucleus and centro-median nucleus), the substantia nigra and in the right subthalamic nucleus (Fig. 2; Table S3 of the Supplementary material).

We did not find any increase in MD or FA in the caudate nucleus. On close examination, it appeared that the nonlinear registration, though grossly matching the caudate nucleus across subjects, was not accurate enough to provide good correspondence of its whole contour. In order to verify these voxel-based findings in the subcortical structures and to test our hypothesis of an increase of MD and FA in the caudate, we then carried out an analysis, insensitive to registration issues, with the manually defined anatomical ROI.

The ROI placed on each individual MD map revealed a bilateral increase in MD values in every SGN including the caudate nucleus, anincrease that was significant except for in the left thalamus (Fig. 2; Table 1). MD was higher by +19% on average in the caudate of the patients, +34% in the putamen, +23% in the ventral striatum and +17% in the pallidum.

FA values were found to be significantly higher in the head and body of the caudate, in the anterior putamen, the pallidum and the right thalamus. More precisely, FA values were increased by +27% in the caudate, +17% in the anterior putamen, +18% in the pallidum and were also increased by +11% in the posterior putamen and +6% in the thalamus (Fig. 2; Table 2).

Analysis of the fibre orientations in the SGN: further in vivo evidence to support selective degeneration in the SGN

Using the anatomical ROI defined in the SGN, we carried out an analysis of the dispersion of the main fibre orientations (PDD) in each structure (Schwartzman et al., 2005).

This analysis revealed a significant decrease in dispersion in the head and body of the caudate, the anterior putamen, the pallidum and the thalamus compared to the control group (Fig. 3). More specifically, the dispersion was on average reduced in the patients by −15% in the caudate, −17% in the putamen, −5% in the ventral striatum, −17% in the pallidum and by −21% in the thalamus.

A whole-brain voxel-wise analysis revealed a significant bilateral reduction in the |*x*| component of the PDD in the patients, exclusively confined to the anterior and posterior putamen and to the pallidum (Fig. 3). Furthermore, we found a significant bilateral increase in the |*y*| and |*z*| components of fibre orientation, almost solely located in the anterior and dorsal lenticular nucleus respectively (Fig. 3).

Table 1
ROI analysis of MD inside the SGN.

SGN	Side	Controls	Patients	*t*-value	*P*-value
		Mean (SE)	Mean (SE)		
Body of the caudate nucleus	R	0.92 (0.04)	1.07 (0.04)	2.30	0.03
Body of the caudate nucleus	L	0.89 (0.06)	1.11 (0.05)	3.79	0.001
Head of the caudate nucleus	R	0.86 (0.02)	1.00 (0.02)	4.76	0.0002
Head of the caudate nucleus	L	0.87 (0.03)	1.03 (0.02)	5.11	$<10^{-4}$
Anterior putamen	R	0.78 (0.02)	1.02 (0.02)	8.51	$<10^{-7}$
Anterior putamen	L	0.79 (0.03)	1.02 (0.02)	6.92	$<10^{-5}$
Posterior putamen	R	0.77 (0.03)	1.09 (0.02)	9.31	$<10^{-7}$
Posterior putamen	L	0.78 (0.03)	1.07 (0.02)	9.05	$<10^{-7}$
Ventral striatum	R	0.84 (0.04)	1.04 (0.03)	7.54	$<10^{-6}$
Ventral striatum	L	0.84 (0.03)	1.03 (0.03)	5.18	$<10^{-4}$
Globus pallidus	R	0.80 (0.02)	0.95 (0.02)	8.28	$<10^{-7}$
Globus pallidus	L	0.81 (0.02)	0.95 (0.02)	4.94	$<10^{-4}$
Thalamus	R	0.83 (0.01)	0.84 (0.01)	2.28	0.03
Thalamus	L	0.81 (0.01)	0.82 (0.01)	1.63	0.12

Adjusted mean MD values (SE) of Huntington's disease patients and controls ($\times 10_{-9}\, m_2.s_{-1}$) and ANCOVA results between the two populations.

Table 2
ROI analysis of FA inside the SGN.

SGN	Side	Controls	Patients	*t*-value	*P*-value
		Mean (SE)	Mean (SE)		
Body of the caudate nucleus	R	0.22 (0.01)	0.27 (0.01)	4.97	$<10^{-4}$
Body of the caudate nucleus	L	0.23 (0.01)	0.30 (0.01)	5.19	$<10^{-4}$
Head of the caudate nucleus	R	0.21 (0.01)	0.26 (0.01)	3.05	0.007
Head of the caudate nucleus	L	0.21 (0.01)	0.27 (0.01)	5.00	0.0001
Anterior putamen	R	0.21 (0.01)	0.24 (0.01)	2.79	0.01
Anterior putamen	L	0.22 (0.01)	0.26 (0.01)	3.00	0.007
Posterior putamen	R	0.24 (0.01)	0.27 (0.01)	1.73	0.10
Posterior putamen	L	0.25 (0.01)	0.28 (0.01)	1.90	0.07
Ventral striatum	R	0.23 (0.01)	0.24 (0.01)	0.83	0.41
Ventral striatum	L	0.25 (0.01)	0.24 (0.01)	−0.67	0.51
Globus pallidus	R	0.35 (0.02)	0.41 (0.01)	2.39	0.03
Globus pallidus	L	0.34 (0.02)	0.41 (0.02)	2.67	0.01
Thalamus	R	0.32 (0.01)	0.34 (0.01)	2.06	0.05
Thalamus	L	0.33 (0.01)	0.35 (0.01)	1.42	0.17

Adjusted mean FA values (SE) between Huntington's disease patients and controls and ANCOVA results.

Analysis of the white matter tracts connecting the SGN: confirmation of the preferential vulnerability of SGN connections in the white matter

We used tractography to reconstruct the virtual white matter tracts coming from or going to each SGN and compared MD values between the HD and control populations for each fibre bundle.

A pathway by diagnosis effect, demonstrating a preferential vulnerability amongst the connections of the SGN, was found highly significant ($P<10^{-6}$). More precisely, among all the virtual fibre bundles, the highest increase in MD was found in the putamino-pallidal projections (+23%). For each SGN, MD values were greater in the striato-pallidal connections compared to other connections (i.e. cortex-striatum, striatum-substantia nigra, thalamus-striatum), this pathway by diagnosis effect being highly significant in the tracts between the putamen and the pallidum (see Fig. 4 and Table S2 of the Supplementary material).

Outside the SGN-SGN connections, the most significant effect was found in the cortical afferents to the putamen, especially to its posterior part i.e. mainly sensori-motor, premotor and prefrontal projections (Lehericy et al., 2004).

Discussion

Although HD is mainly considered to be a subcortical disease, there is no clear consensus on whether all the deep grey matter loss is directly related to the original death of the medium-size spiny neurons of the striatum. It is essential to be capable of characterising *in vivo* such preferential degeneration as it would give a better insight into the evolving process of this neurodegenerative disease. To question this matter, we have used several distinct diffusion imaging measures, some of them being applied for the very first time to patients with neurodegenerative pathology. Complementary voxel-wise and ROI approaches were carried out, to ensure that the results obtained were not possibly driven by some residual mis-registration when warping the diffusion images into a common standard space. All results–measures of MD, FA, PDD dispersion and white matter tractography–converged to demonstrate the selective degeneration of connections in the subcortical grey nuclei, degeneration that is likely to originate with the death of the striatal spiny neurons.

Increases in MD have often already been reported in previous studies on age- or disease-related neurodegeneration (Moseley, 2002; Bozzali and Cherubini, 2007). In line with our findings, two previous

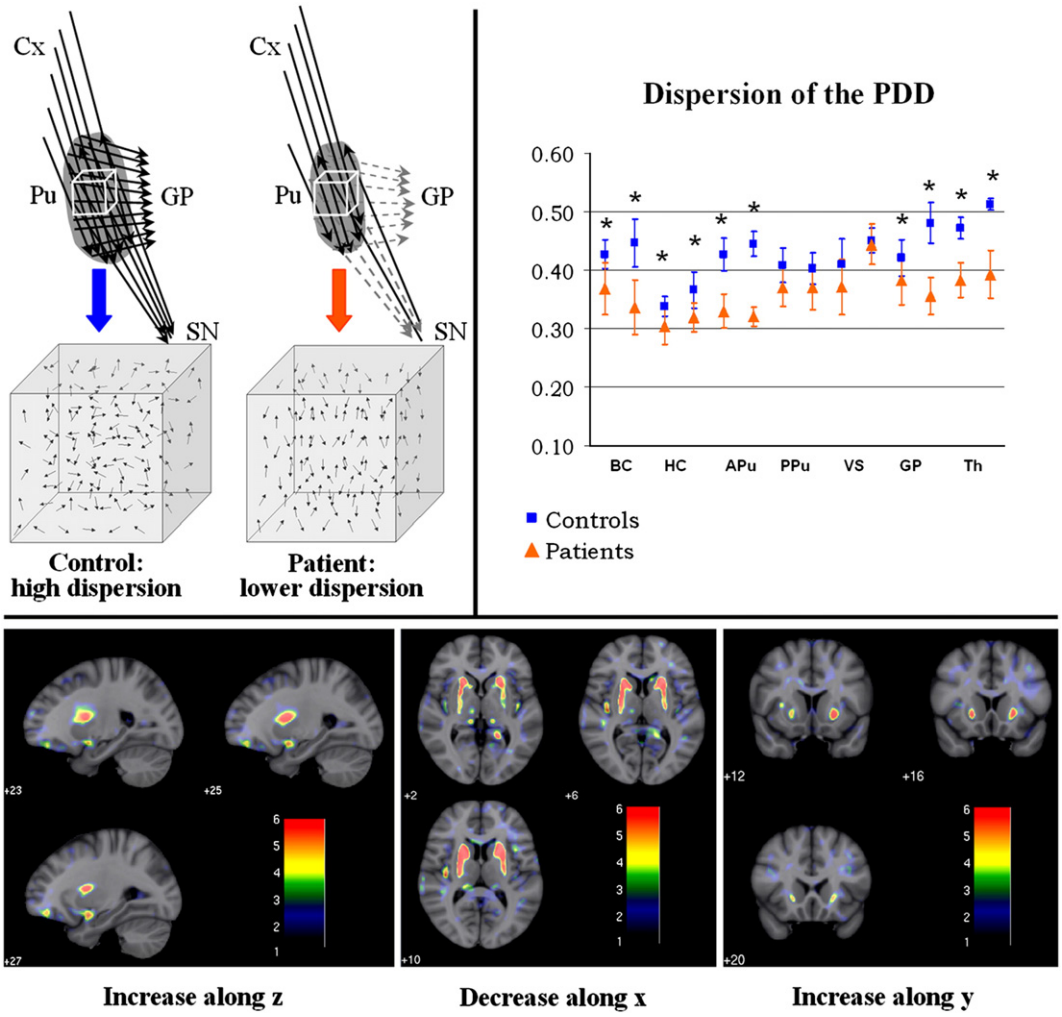

Fig. 3. ROI and voxel-wise ANCOVA results on the main fibre orientations (PDD). Top left, illustrative example for the increase of anisotropy: schematic coronal views of a control and HD patient putamen, their afferents and efferents: various connections are selectively affected by the degenerative process in the HD patient; this preferential degeneration should have an impact on the PDD inside the structure, which we have schematised in the enlarged cubic views of the putamen. Top right, ROI analysis of the mean dispersion values (±SE) of the PDD in each SGN indeed reveals a decrease of this dispersion in the patients.* = significant. Bottom, voxel-wise results of the |x|, |y| and |z| components of the PDD show as predicted a decrease in |x| and an increase in |y| and |z|.

DTI studies using ROI analyses have shown higher MD values in the caudate and the putamen of HD patients (Mascalchi et al., 2004; Seppi et al., 2006), whilst one study only found it in the putamen (Rosas et al., 2006). More precisely, one of the studies showed an increase of +24% in the caudate and of +36% in the putamen which is in good agreement with our results in the neostriatum (+19% and +34% respectively) (Mascalchi et al., 2004). The increase found in this study is slightly greater than the one we established probably because it was observed in patients at more advanced stages of the disease than the ones included in our study. This striatal MD increase is likely to be caused by the expansion of the extracellular space corresponding to a decrease in membrane density due to cell degeneration, which is in accordance with the volume loss in each sub-region of the striatum previously observed in these patients (Douaud et al., 2006). The higher MD values observed in the pallidum confirmed the results of two recent studies (Seppi et al., 2006; Rosas et al., 2006). This increase may either be imputable to the sole loss of the projections from striatal spiny neurons, or to neuronal shrinking or depletion within the pallidum itself (Wakai et al., 1993).

Furthermore, we have found that FA values were increased in the caudate, the putamen and the pallidum. Two studies have reported an increased anisotropy in the lenticular nucleus but did not find any significant FA differences in the caudate, which should logically present a similar pattern to that observed in the putamen (Rosas et al., 2006; Kloppel et al., 2008). In contrast with the MD findings, the increased FA found in the deep grey matter is an unusual result. To our knowledge, there are only four studies showing such a result: one in multiple sclerosis (Ciccarelli et al., 2001), one in ageing (Furutani et al., 2005) and two in HD (Rosas et al., 2006; Kloppel et al., 2008). By the admission of the authors of the most recent study (Kloppel et al., 2008), the "FA increases (found) in grey matter are difficult to interpret". In this study, we suggested that the selective loss of some of the subcortical connections targeted by the degenerative process–i.e., mainly the striato-pallidal projections at this early stage of the disease (Reiner et al., 1988; Albin et al., 1992; Mitchell et al., 1999; Deng et al., 2004)–may turn the striatum into a seemingly more organized structure.

We were able to test this hypothesis using a novel approach, never applied so far to clinical studies, which aims at examining the DTI data differently by studying the main fibre orientation depicted by the principal diffusion direction (Schwartzman et al., 2005). This ROI analysis revealed that the dispersion of the PDD was reduced in the neostriatum and the pallidum of the patients, unambiguously characterising a preferential loss of connections along specific radiating directions from these structures while some others were comparatively spared. PDD dispersion in the putamen also happened to

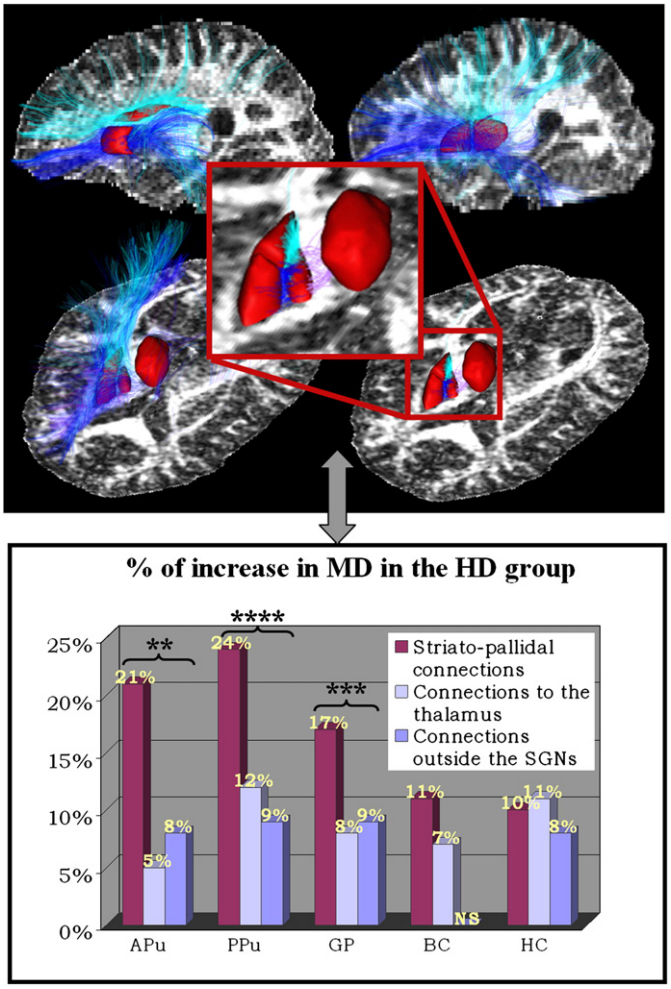

Fig. 4. Analyses of the virtual reconstructed white matter tracts from the SGN show greater abnormalities in the striato-pallidal connections. Left, virtual tracts reconstructed from the right caudate nucleus (head and body) and the right putamen (anterior and posterior) as well as tracts from the right putamen and pallidum before and after fragmenting and re-labeling the fibre bundles according to the various subregions of the SGN. Right, the percentage of increase in MD in the HD population compared to the control group: striato-pallidal connections are the more affected compared to the other connections. ** = $P<0.005$; *** = $P<0.0001$; **** = $P<10^{-8}$.

provide the highest sensitivity for correctly diagnosing patients (93%), compared with MD in the putamen (86%) or FA in the caudate nucleus (71%). As a corollary, we also more specifically interrogated our hypothesis by looking at the |*x*|, |*y*| and |*z*| components of the main fibre orientations. In the HD population, we predicted a very focal shift in the PDD away from the medio-lateral orientation (*x*-axis) of the putamino-pallidal connections towards the antero-posterior (*y*-axis) and the dorsal-ventral (*z*-axis) orientations of the cortical-putaminal projections (Parent and Parent, 2006). However, we could not make any assumptions about the organization of the fibres inside the caudate nucleus as the cortico-striatal projections to this structure have a less distinct organization compared with the striato-pallidal pathways. And indeed as predicted, a whole-brain voxel-wise analysis revealed a decrease in the |x| component concurrent with an increase in the |*y*| and |*z*| components in the lenticular nucleus and *only* in this structure. This reflects the fact that the cortico-putaminal connections are relatively spared by the degenerative process at this stage of the disease compared to the putamino-pallidal pathways. This result can be compared to a similar ROI-based finding in Wallerian degeneration by Pierpaoli et al., who found a significant decrease of the PDD along the *z* axis characterising damages to the descending motor pathways in the rostral pons concurrent to an increase of the PDD along the *x* axis, showing that the transverse pontine fibres became the dominant pathway in this region (Pierpaoli et al., 2001).

In the white matter itself, the hypothesis of a preferential loss of some of the striatal connections was further supported by our tractography results, which precisely showed a significant increase in MD in the striato-pallidal projections. The biggest effect was found in the projection from the putamen to the pallidum (+23% on average), while the other connections of the putamen (with the substantia nigra and the cortex) and the pallidum (with the thalamus and the subthalamic nucleus) showed a more moderate increase in mean diffusivity (+9%). Outside the subcortico-subcortical connections, the most significant effect was found in the cortical afferents to the putamen, remarkably coinciding with the white matter abnormalities located around the central sulcus revealed with the voxel-wise analysis of MD (see Fig. 5 for example in one subject). These MD differences in the corticostriatal pathways are in line with previous imaging and *post mortem* reports in both HD patients and animal model showing loss in the cerebral white matter and degeneration of the pyramidal cells the primary motor cortex (MacDonald and Halliday, 2002; Rosas et al., 2003; Fennema-Notestine et al., 2004; Cepeda et al., 2007). We further wanted to test if this modification of the mean diffusivity in the cortico-striatal projections was related to a possible loss of white matter quantifiable with a voxel-based morphometry (VBM) white matter analysis. We therefore performed the optimised white matter VBM protocol (Good et al., 2001) that showed a loss of deep white matter localised exclusively around the basal ganglia (see comments and Fig. S5 of the Supplementary material). It did not reveal any loss in the corona radiata after correction for multiple comparisons. This emphasizes that the MD index is sensitive to microstructural alterations of fibre bundles between the sensori-motor, premotor and prefrontal cortices and the striatum, before this micro-structural change develops into macro-structural loss measurable by VBM analyses.

Voxel-based DTI analyses, which require no prior knowledge of the location of diffusion abnormalities, also allowed us to identify the thalamic nuclei targeted by the degenerative process and to reveal other subcortical microstructural alterations in the substantia nigra and the right subthalamic nucleus. Indeed, we found significantly higher MD and FA values in the ventro-lateral and the centro-median nuclei of the patients. Thalamic atrophy previously reported in these patients may therefore be confined to these two nuclei, which could explain the moderate volume loss in this subcortical structure (−16%) (Douaud et al., 2006). As both ventro-lateral and centro-median nuclei are part of the cortico-striato-thalamo-cortical loop, these microstructural alteration and atrophy are most likely related to primary striatal injury (Parent and DeBellefeuille, 1983; Sidibe et al., 1997; McFarland and Haber; 2002; Behrens et al., 2003). We also found a significant FA increase in the substantia nigra that may be driven by a selective deficit of striatal afferents and is in good agreement with the atrophy found previously in this structure (Douaud et al., 2006). Finally, while conventional T1-weighted MRI analyses have so far failed to reveal any alteration of the subthalamic nucleus, we were finally able to demonstrate an FA increase in this structure that completes the cortico-subcortico-cortical circuitry (Hamani et al., 2004).

What have we learnt in vivo about the subcortical pathophysiological impact of HD?

The combined analyses of various DTI indices in HD therefore converge to provide meaningful information about the pathophysiological damage occurring in the subcortical regions of the brain. Interestingly, all subcortical grey matter structures involved in the cortico-striato-thalamo-cortical loops show microstructural abnormalities: the striatum, the pallidum, the ventro-lateral and the centro-median nuclei of the thalamus, the subthalamic nucleus and finally

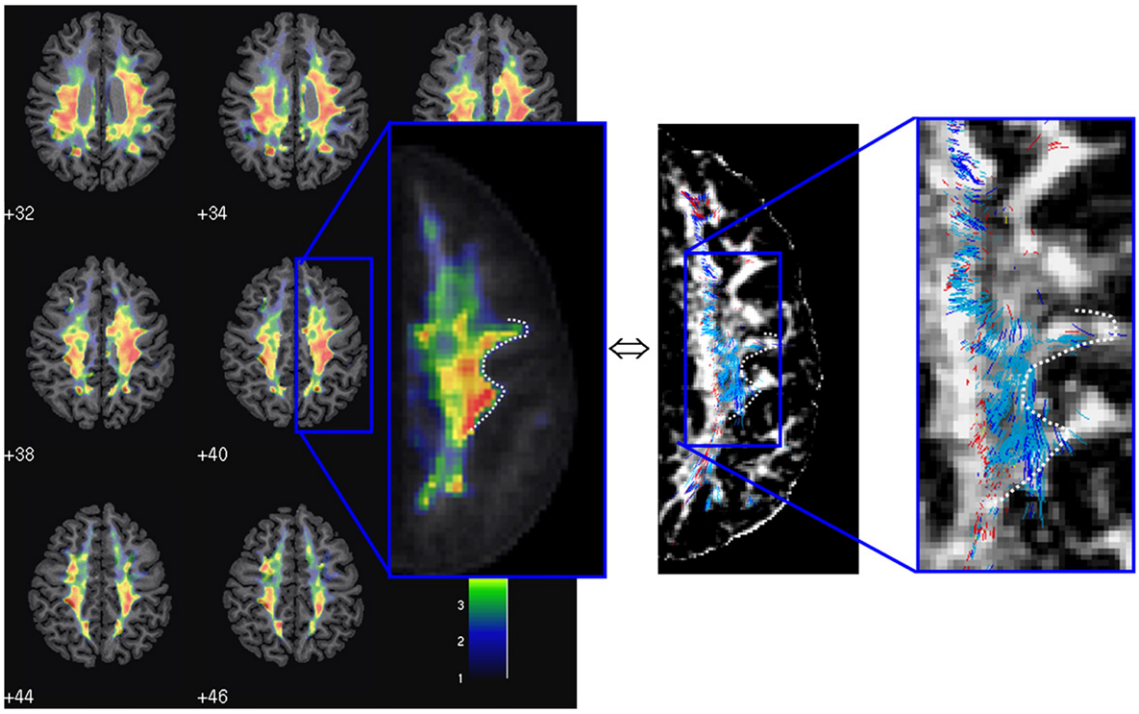

Fig. 5. Voxel-based analysis of MD and corresponding striatal tractography in the white matter. Left, *t*-map of MD differences at $z = +40$ mm (patients > controls). Right, results of the striatal tractography of a control: cortical afferents projecting onto the body of the caudate (red), the anterior (dark blue) and posterior (light blue) putamen. The enlarged view shows that the virtual fibre tracts appear to mainly project to the posterior putamen in the area corresponding to where the increase of MD is found the most significant with the voxel-based analysis.

the substantia nigra. The only point of convergence of these loops being the striatum, it therefore seems probable that these abnormalities have as common origin the dramatic loss of striatal medium-size spiny neurons. All the subcortical white matter connections implicated in the cortico-striato-thalamo-cortical circuitry also show an increase in MD, reinforcing the assumption of a primary degeneration in the striatum.

Furthermore, voxel-based analysis of MD is able to reveal microstructural abnormalities in the white matter proximal to premotor and primary sensorimotor cortices, likely representing cortical projections to the posterior putamen. As the centro-median thalamic nucleus, sending back its efferents to the sensorimotor territories of the striatum and to the motor and premotor cortical areas, is predominantly involved in the motor basal ganglia-thalamo-cortical loop (Alexander et al., 1990; Parent and Parent, 2005), this altogether suggests that the motor subcortical loop is the most affected by the degenerative process at this stage of the disease.

A crucial finding of this study is the *in vivo* characterisation of a selective degeneration of fibre tracts in subcortical regions. In the white matter, it is characterised by a massive increase in the mean diffusivity of the striato-pallidal connections (even more particularly between the putamen and the pallidum), an increase that was substantially bigger than for other striatal and pallidal connections. In the grey matter, this preferential loss of some fibre tracts is characterised by an increase in anisotropy. To find such an increase in a pathological study is a singular result. By analysing the dispersion of the fibre orientations in the subcortical grey nuclei, we have been able to demonstrate that this increase was related to a selective degeneration that had only been demonstrated *post mortem* so far (Reiner et al., 1988; Albin et al., 1992; Mitchell et al., 1999; Deng et al., 2004). This result is unprecedented and provides a solid answer to the few studies that found increased anisotropy in subcortical grey matter (Ciccarelli et al., 2001; Furutani et al., 2005; Rosas et al., 2006; Kloppel et al., 2008). Above all, it offers the exciting perspective of being able to study *in vivo* the selective impact of HD in large population of patients and to follow the progressive degeneration in the subcortical structures and their connections, progression that *post mortem* studies do not permit by definition. The ability of DTI to uncover this preferential impact of the disease on some neuronal and axonal populations may represent in the future a precious surrogate marker to assess and monitor the impact of experimental therapies such as cell transplantation or neuroprotective gene therapy (Bachoud-Levi et al., 2000; McBride et al., 2006).

Finally, the techniques we have outlined in this manuscript are not limited in their scope to HD. They can as such provide significant insight into any neurodegenerative disorder for which some neuronal populations or connections are selectively targeted over others including multiple sclerosis (Ciccarelli et al., 2001), Parkinson's disease (Yoshikawa et al., 2004) or Alzheimer's disease (Ringman et al., 2007).

Acknowledgments

We thank Drs. Jean-François Mangin and Edouard Duchesnay at the SHFJ for providing helpful advices. We would also like to thank Drs. Jill O'Reilly and Michael Chappell for their help with editing the English grammar. We are finally grateful to Prof. Stephen Smith for being magnanimous concerning the time spent writing this manuscript. This study is part of the MIG-HD program and is supported by the Délégation Régionale à la Recherche Clinique (PHRC P001106), the Association Française contre les Myopathies and the Etablissement Français des Greffes. Drs. Timothy Behrens and Saad Jbabdi have been supported by the Dr Hadwen Trust for Humane Research.

Appendix A. Supplementary data

Supplementary data associated with this article can be found, in the online version, at doi:10.1016/j.neuroimage.2009.03.044.

References

Albin, R.L., Reiner, A., Anderson, K.D., L. St., Dure, Handelin, B., Balfour, R., et al., 1992. Preferential loss of striato-external pallidal projection neurons in presymptomatic Huntington's disease. Ann. Neurol. 31, 425–430.

Alexander, G.E., Crutcher, M.D., DeLong, M.R., 1990. Basal ganglia-thalamocortical circuits: parallel substrates for motor, oculomotor, "prefrontal" and "limbic" functions. Prog. Brain Res. 85, 119–146.

Aylward, E.H., Sparks, B.F., Field, K.M., Yallapragada, V., Shpritz, B.D., Rosenblatt, A., et al., 2004. Onset and rate of striatal atrophy in preclinical Huntington disease. Neurology 63, 66–72.

Bachoud-Levi, A.C., Remy, P., Nguyen, J.P., Brugieres, P., Lefaucheur, J.P., Bourdet, C., et al., 2000. Motor and cognitive improvements in patients with Huntington's disease after neural transplantation. Lancet 356, 1975–1979.

Beaulieu, C., 2002. The basis of anisotropic water diffusion in the nervous system—a technical review. NMR Biomed. 15, 435–455.

Behrens, T.E., Johansen-Berg, H., Woolrich, M.W., Smith, S.M., Wheeler-Kingshott, C.A., Boulby, P.A., 2003. Non-invasive mapping of connections between human thalamus and cortex using diffusion imaging. Nat. Neurosci. 6, 750–757.

Bozzali, M., Cherubini, A, 2007. Diffusion tensor MRI to investigate dementias: a brief review. Magn. Reson. Imaging 25, 969–977.

Cepeda, C., Wu, N., Andre, V.M., Cummings, D.M., Levine, M.S., 2007. The corticostriatal pathway in Huntington's disease. Prog. Neurobiol. 81, 253–271.

Ciccarelli, O., Werring, D.J., Wheeler-Kingshott, C.A., Barker, G.J., Parker, G.J., Thompson, A.J., 2001. Investigation of MS normal-appearing brain using diffusion tensor MRI with clinical correlations. Neurology 56, 926–933.

Cointepas Y., Mangin J.F., Garnero L., Poline J.B., Benali H. BrainVISA: Software platform for visualization and analysis of multi-modality brain data. In *Proc. 7th HBM*, Brighton, United Kingdom, pages S98, 2001. Keyword(s): Computer Science.

Deng, Y.P., Albin, R.L., Penney, J.B., Young, A.B., Anderson, K.D., Reiner, A., 2004. Differential loss of striatal projection systems in Huntington's disease: a quantitative immunohistochemical study. J. Chem. Neuroanat. 27, 143–164.

Douaud, G., Gaura, V, Ribeiro, M.J., Lethimonnier, F., Maroy, R., Verny, C., 2006. Distribution of grey matter atrophy in Huntington's disease patients: a combined ROI-based and voxel-based morphometric study. Neuroimage 32, 1562–1575.

Duchesnay, E., Roche, A., Rivière, D., Papadopoulos-Orfanos, D., Cointepas, Y., Mangin, J.F., 2004. Population classification based on structural morphometry of cortical sulci. In *Proc. 2th Proc. IEEE ISBI*, Arlington, VA, pp. 1276–1279 (Apr.).

Fennema-Notestine, C., Archibald, S.L., Jacobson, M.W., Corey-Bloom, J., Paulsen, J.S., Peavy, G.M., 2004. In vivo evidence of cerebellar atrophy and cerebral white matter loss in Huntington disease. Neurology 63, 989–995.

Furutani, K., Harada, M., Minato, M., Morita, N., Nishitani, H., 2005. Regional changes of fractional anisotropy with normal aging using statistical parametric mapping (SPM). J. Med. Invest. 52, 186–190.

Genovese, C.R., Lazar, N.A., Nichols, T., 2002. Thresholding of statistical maps in functional neuroimaging using the false discovery rate. Neuroimage 15 (4), 870–878 (Apr.).

Good, C.D., Johnsrude, I.S., Ashburner, J, Henson, R.N., Friston, K.J., Frackowiak, R.S., 2001. A voxel-based morphometric study of ageing in 465 normal adult human brains. Neuroimage 14, 21–36.

Graveland, G.A., Williams, R.S., DiFiglia, M., 1985. A Golgi study of the human neostriatum: neurons and afferent fibers. J. Comp. Neurol. 234, 317–333.

Hamani, C., Saint-Cyr, J.A., Fraser, J., Kaplitt, M., Lozano, A.M., 2004. The subthalamic nucleus in the context of movement disorders. Brain 127, 4–20.

Jernigan, T.L., Salmon, D.P., Butters, N, Hesselink, JR, Cerebral structure on, MRI, 1991. Part II: specific changes in Alzheimer's and Huntington's diseases. Biol. Psychiatry 29, 68–81.

Jezzard, P., Balaban, R.S., 1995. Correction for geometric distortion in echo planar images from B0 field variations. Magn. Reson. Med. 34, 65–73.

Jones, D.K., Symms, M.R., Cercignani, M., Howard, R.J., 2005. The effect of filter size on VBM analyses of DT-MRI data. Neuroimage 26, 546–554.

Kloppel, S., Draganski, B., Golding, C.V., Chu, C., Nagy, Z., Cook, P.A., et al., 2008. White matter connections reflect changes in voluntary-guided saccades in pre-symptomatic Huntington's disease. Brain 131, 196–204.

Lehericy, S., Ducros, M., Van de Moortele, P.F., Francois, C., Thivard, L., Poupon, C, 2004. Diffusion tensor fiber tracking shows distinct corticostriatal circuits in humans. Ann. Neurol. 55, 522–529.

Macdonald, V., Halliday, G., 2002. Pyramidal cell loss in motor cortices in Huntington's disease. Neurobiol. Dis. 10, 378–386.

Mangin, J.F., Poupon, C., Clark, C., Le Bihan, D., Bloch, I., 2002. Distortion correction and robust tensor estimation for MR diffusion imaging. Med. Image Anal. 6, 191–198.

Mascalchi, M., Lolli, F., Della Nave, R., Tessa, C., Petralli, R., Gavazzi, C, 2004. Huntington disease: volumetric, diffusion-weighted, and magnetization transfer MR imaging of brain. Radiology 232, 867–873.

McBride, J.L., Ramaswamy, S., Gasmi, M., Bartus, R.T., Herzog, C.D., Brandon, E.P., et al., 2006. Viral delivery of glial cell line-derived neurotrophic factor improves behavior and protects striatal neurons in a mouse model of Huntington's disease. Proc. Natl. Acad. Sci. U. S. A. 103, 9345–9350.

McFarland, N.R., Haber, S.N, 2002. Thalamic relay nuclei of the basal ganglia form both reciprocal and nonreciprocal cortical connections, linking multiple frontal cortical areas. J. Neurosci. 22, 8117–8132.

Mitchell, I.J., Cooper, A.J., Griffiths, M.R., 1999. The selective vulnerability of striatopallidal neurons. Prog. Neurobiol. 59, 691–719.

Moseley, M., 2002. Diffusion tensor imaging and aging—a review. NMR Biomed. 15, 553–560.

Parent, A., De Bellefeuille, L., 1983. The pallidointralaminar and pallidonigral projections in primate as studied by retrograde double-labeling method. Brain Res. 278, 11–27.

Parent, M., Parent, A., 2005. Single-axon tracing and three-dimensional reconstruction of centre median-parafascicular thalamic neurons in primates. J. Comp. Neurol. 481, 127–144.

Parent, M., Parent, A., 2006. Single-axon tracing study of corticostriatal projections arising from primary motor cortex in primates. J. Comp. Neurol. 496, 202–213.

Perrin, M., Poupon, C., Cointepas, Y., Rieul, B., Golestani, N., Pallier, C., 2005. Fiber tracking in q-ball fields using regularized particle trajectories. Inf. Process Med. Imaging 19, 52–63.

Pierpaoli, C., Basser, P.J., 1996. Toward a quantitative assessment of diffusion anisotropy. Magn. Reson. Med. 36, 893–906.

Pierpaoli, C., Barnett, A, Pajevic, S., Chen, R., Penix, L.R., Virta, A., et al., 2001. Water diffusion changes in Wallerian degeneration and their dependence on white matter architecture. Neuroimage 13, 1174–1185.

Reiner, A., Albin, R.L, Anderson, K.D., D., Amato, C.J., Penney, J.B., Young, A.B., 1988. Differential loss of striatal projection neurons in Huntington disease. Proc. Natl. Acad. Sci. U. S. A. 85, 5733–5737.

Ringman, J.M., O., Neill, J., Geschwind, D., Medina, L., Apostolova, L.G, Rodriguez, Y., et al., 2007. Diffusion tensor imaging in preclinical and presymptomatic carriers of familial Alzheimer's disease mutations. Brain 130, 1767–1776.

Rosas, H.D., Koroshetz, W.J., Chen, Y.I., Skeuse, C., Vangel, M., Cudkowicz, M.E., et al., 2003. Evidence for more widespread cerebral pathology in early HD: an MRI-based morphometric analysis. Neurology 60, 1615–1620.

Rosas, H.D., Tuch, D.S., Hevelone, N.D., Zaleta, A.K., Vangel, M., Hersch, S.M., 2006. Diffusion tensor imaging in presymptomatic and early Huntington's disease: selective white matter pathology and its relationship to clinical measures. Mov. Disord. 21, 1317–1325.

Seppi, K., Schocke, M.F., Mair, K.J., Esterhammer, R., Weirich-Schwaiger, H., Utermann, B., 2006. Diffusion-weighted imaging in Huntington's disease. Mov. Disord. 21, 1043–1047.

Shoulson, I., Fahn, S., 1979. Huntington disease: clinical care and evaluation. Neurology 29, 1–3.

Schwartzman, A., Dougherty, R.F, Taylor, J.E., 2005. Cross-subject comparison of principal diffusion direction maps. Magn. Reson. Med. 53, 1423–1431.

Sidibe, M., Bevan, M.D., Bolam, J.P., Smith, Y., 1997. Efferent connections of the internal globus pallidus in the squirrel monkey: I. Topography and synaptic organisation of the pallidothalamic projection. J. Comp. Neurol. 382, 323–347.

Stejskal, E.O., Tanner, J.E., 1965. Spin diffusion measurements: spin echoes in the presence of a time-dependent field gradient. J. Chem. Phys. 42 (1), 288–292 (January 1).

Vonsattel, J.P., Myers, R.H., Stevens, T.J., Ferrante, R.J., Bird, E.D., Richardson Jr., E.P., 1985. Neuropathological classification of Huntington's disease. J. Neuropathol. Exp. Neurol. 44, 559–577.

Wakai, M., Takahashi, A., Hashizume, Y., 1993. A histometrical study on the globus pallidus in Huntington's disease. J. Neurol. Sci. 119, 18–27.

Yoshikawa, K., Nakata, Y., Yamada, K., Nakagawa, M., 2004. Early pathological changes in the parkinsonian brain demonstrated by diffusion tensor MRI. J. Neurol. Neurosurg. Psychiatry 75, 481–484.